Intermediates of the S_3 State of the Oxygen-Evolving Complex of Photosystem II†

Nikolaos Ioannidis,*,‡ Jonathan H. A. Nugent,§ and Vasili Petrouleas*,‡

Institute of Materials Science, NCSR "Demokritos", 15310 Aghia Paraskevi Attikis, Greece, and Department of Biology, University College London, Gower Street, London WC1E 6BT, U.K.

Received November 29, 2001; Revised Manuscript Received June 3, 2002

ABSTRACT: The S_3 state of the water-oxidizing complex (WOC) of photosystem II (PSII) is the last state that can be trapped before oxygen evolution occurs at the transient S_4 state. A number of EPR-detectable intermediates are associated with this critical state. The preceding paper examined mainly the decay of S_3 at cryogenic temperatures leading to the formation of a proton-deficient configuration of S_2 termed S_2'. This second paper examines all intermediates formed by the near-IR light (NIR) excitation of the S_3 state and compares these with the light-excitation products of the S_2' state. The rather complex set of observations is organized in a comprehensive flowchart, the central part of which is the $S_3...Q_A^-$ state. This state can be converted to various intermediates via two main pathways: (A) Excitation of S_3 by NIR light at temperatures below 77 K results presumably in the formation of an excited S_3 state, S_3*, which decays via either of two pathways. Slowly at liquid helium temperatures but much faster at 77 K, S_3* decays to an EPR-silent state, denoted S_3'', which by raising the temperature to ca. 190 K converts to a spin configuration of the Mn cluster, characterized by $g = 21$, 3.7 in perpendicular and $g = 23$ in parallel mode EPR, denoted S_3'. Upon further warming to 220 K, S_3' relaxes to the untreated S_3 state. Below about 77 K and more favorably at liquid helium temperatures, an alternative pathway of S_3* decay via the metallo−radical intermediate $S_2'Z^{\bullet}...Q_A^-$ can be traced. This leads to the metastable state $S_2'Z...Q_A$ via charge recombination. $S_2'Z^{\bullet}$ is characterized by a split-radical signal at $g = 2$, while all S_2' transients are characterized by the same $g = 5/2.9$ ($S = {}^7/_2$) configuration of the Mn cluster with small modifications, reflecting an influence of the tyr Z oxidation state on the crystal-field symmetry at the Mn cluster. (B) $S_2'...Q_A$ can be reached alternatively by the slow charge recombination of S_3 and Q_A^- at 77 K. White-light illumination of $S_2'...Q_A$ below about 20 K results in charge separation, reforming the intermediate $S_2'Z^{\bullet}...Q_A^-$. Thermally activated branches to the main pathways are also described, e.g., at elevated temperatures tyr $Z^{\bullet}$ reoxidizes S_2' to the S_3 state. The above observations are discussed in terms of a molecular model of the S_3 state of the OEC. Main aspects of the model are the following. Intermediates, isoelectronic to S_3, are attributed to the NIR-induced translocation of the positive hole to different Mn ligands, or to tyr Z. On the basis of a comparison of the electron-donating efficiency of tyr Z and tyr D at cryogenic temperatures, it is inferred that the Mn cluster acts as the main proton acceptor from tyr Z. Water associated with the Mn cluster is assumed to be in hydrogen-bonding equilibrium with tyr Z, and an array comprising this water and adjacent water (or OH or O) ligands to Mn followed by a sequence of proton acceptors is proposed to act as an efficient proton translocation pathway. Oxidation of the tyrosine by P_{680}^+ repels protons to and out from the Mn cluster. This proposed role of tyr Z in the water-splitting process is described as a proton repeller/electron abstractor.

Photosystem II, PS II[1], is a membrane-bound protein complex which catalyses the photosynthetic water splitting process in plants, algae, and cyanobacteria. The core of PS II, where the main photochemistry occurs, consists of two polypeptide chains, D1 and D2, on which a number of electron transport cofactors are attached (*1*). The chlorophyll species P_{680} is the site where light excitation induces the primary charge separation. Upon absorption of one photon, one electron is transferred from P_{680} to a pheophytin molecule. The latter reduces the acceptor side, which is made up of a plastoquinone A, Q_A (a one-electron carrier), a nonheme iron atom (when preoxidized the iron acts as an

† This work was supported in part by the Grant ERBFMRX-CT980214 and by the Greek Secretariat of Research and Technology (PENED 99ED75). Financial support to J.H.A.N. was from the U.K. Biotechnology and Biological Sciences Research Council.

* Corresponding authors. V. Petrouleas: tel, +301 650-3344; fax, +301 6519430; e-mail, vpetr@ims.demokritos.gr. N. Ioannidis: tel, +301 650-3312; fax, +301 6519430; e-mail, nioannid@ims.demokritos.gr.

‡ NCSR "Demokritos".

§ University College London.

[1] Abbreviations: PSII, Photosystem II; OEC, oxygen-evolving complex; WOC, water-oxidising complex; BBY membranes, thylakoid membrane fragments enriched in PSII; S states S_0... S_4, oxidation states of the water-oxidising complex; tyr Z, Z, or Y_Z and tyr D, D, or Y_D, the fast and slow tyrosine electron donors of PSII; signal II, the unperturbed EPR spectrum of either of the two tyrosines, a measure of oxidized tyr D under the present conditions; broad or split $g \sim 2$ signal, a broadened radical signal; Q_A and Q_B, the primary and secondary plastoquinone electron acceptors of PSII; cw EPR, continuous-wave electron paramagnetic resonance; NIR light, near-infrared light; MES, 2-[N-Morpholineethanesulfonic acid]; chl, chlorophyll; EtOH, ethanol; MeOH, methanol; XAS, X-ray absorption spectroscopy; XANES, X-ray absorption near-edge structure.

10.1021/bi0159940 CCC: $22.00
Published on Web 07/02/2002

additional electron acceptor), and plastoquinone B, Q_B (a two-electron and two-proton carrier) (*2*). P_{680}^+ oxidizes a redox active tyrosine, tyr Z, which in turn, oxidizes the Mn complex. The Mn complex (believed to be a tetra nuclear cluster) and tyr Z comprise what is termed the oxygen-evolving complex (OEC) or water-oxidizing complex (WOC) (for recent reviews, see refs *3*−*6*). For every four photons absorbed by P_{680}, two molecules of water are oxidized to molecular oxygen by the OEC, and two molecules of Q_B are reduced to Q_BH_2. The OEC cycles through five redox states denoted S_i, $i = 0-4$. Oxygen evolution occurs during the S_3-to-S_0 transition (with the S_4 being a transient state). S_0, which is the lowest active oxidation state of the complex, is slowly oxidized in the dark by the distant tyr D, to the dark-stable state, S_1.

A number of insightful but different models have been proposed in an effort to simulate critical parts of the water-splitting mechanism (*7*−*24*). The models make use of information derived from spectroscopic studies (mainly electron paramagnetic resonance, EPR, and X-ray absorption spectroscopy, XAS) and synthetic chemistry but are naturally limited by the absence of high-resolution information on the 3D structure of the OEC. The recent crystallization and X-ray structure determination of PSII at 3.8 Å resolution (*25*) promises significant advances in this direction. An important parallel goal is the trapping and study of key intermediates and particularly of transients associated with the higher S states.

EPR spectroscopy has been vital to the study of the OEC. Characteristic EPR signals (reviewed briefly in the companion paper, *26*) have been detected now for all active S states (with the exception of the transiently formed S_4). The spectra provide valuable information on steady states but limited insights on mechanistically important S-state intermediates. A natural intermediate of the S-state advancement is oxidized tyr Z, and considerable effort has been devoted in recent years to the trapping of this species. Of particular significance are the broadened radical signals observed following treatments that inhibit advancement to the S_3 state (*27*−*35*). These signals have been attributed to the state $S_2Z^\bullet$ (*10*, *32*−*36*). Theoretical simulations implied a close proximity of tyr Z to the Mn cluster (*37*−*40*), close enough perhaps to have a direct role in the water splitting process as a proton/electron or hydrogen-atom abstractor from water bound to the Mn cluster (*5*, *10*−*12*). The X-ray crystallography suggests a 7 Å closest distance between tyrosine and the Mn cluster (*25*). The trapping of oxidized tyrosine intermediates in oxygen-evolving preparations has been considered to be unlikely, due to the short lifetime of oxidized tyr Z. However, Nugent et al. (*41*) observed a broadened radical signal reminiscent of the $S_2Z^\bullet$ signals seen in inhibited preparations. A similar signal was observed in a separate, more recent study by Ioannidis and Petrouleas, following near-IR (NIR) light excitation at liquid-helium temperatures, of oxygen-evolving samples that were trapped in the S_3 state (*42*). The NIR sensitivity is an unusual property of the Mn cluster observed first in the S_2 state (*43*, *44*). NIR excitation of S_2 at cryogenic temperatures results in the conversion of the $S = {}^1/_2$ multiline state of the complex to the $g = 4$ form via an intermediate $S \geq {}^5/_2$ state. This is attributed to either charge transfer among the Mn ions or light-induced changes in the spin of the Mn cluster (*43*, *44*).

The observation of new transients in untreated PSII (*26*, *41*−*42*, *45*) gives significant new information on the electronic structure of the complex. More than this, it is possible that certain of the transients represent true intermediates of the catalytic mechanism. NIR excitation of S_3 at cryogenic temperatures speeds up charge recombination and leads to the formation of the modified S2 state, S_2'. Presumably, NIR excitation leads to charge transfer from the Mn to tyr Z forming the transient species $S_2'Z^\bullet$. We extend these studies in the present paper and examine the main pathways of decay of the NIR-excited S_3 state. Comparison is also made with the white-light-excitation products of S_2'. The results offer significant new insights into the equilibria among excited S_3 state transients, tyr Z, and S_2. The rather complex observations are organized in a flowchart and combined into a molecular model at the end of the paper.

MATERIALS AND METHODS

PSII-enriched thylakoid membranes were isolated from market spinach by standard procedures (*46*, *47*) with some modifications. Samples for EPR measurements were suspended in 0.4 M sucrose, 15 mM NaCl, 40 mM MES, pH 6.5, at 6−8 mg chl/mL (5 mm EPR tubes) and stored in liquid nitrogen until use.

Entrapment of the S_3-state was achieved as previously described (*42*), but with the following modification. BBY samples with preoxidized nonheme iron, initially kept at 4 °C in darkness, were rapidly transferred into a −30 °C precooled acetone bath under illumination, illuminated for 3 min, and finally placed in liquid nitrogen. For this purpose, white light from a 340 W projection lamp, filtered through a solution of $CuSO_4$, was used. This procedure yielded approximately 50−60% S_3 and 50−40% S_2, measured by monitoring the yield of the EPR signals from the S_2 state. The NIR excitation in addition to the effects on the S_3 state produced changes in the S_2 signals, as has been detailed in (*43*, *44*). In the absence of EtOH, these changes are smaller and did not interfere significantly with the changes of the S_3 signals.

Excitation of the S_3 state by near-infrared light was performed at 4.2 K. The same light source was used, but the light was filtered by a 3 mm RG715 SCHOTT filter immersed in water. Illumination with white light at 4.2 K was done in the same manner, but the projector light was filtered by a 3 mm BG-39 SCHOTT filter immersed in a $CuSO_4$ solution. The duration of illuminations was, unless otherwise stated, 3 min intermittently in 15 s intervals to avoid heating of the sample.

At the end of experiments, samples were dark-adapted for typically 60 min at 4 °C, or 30 min at 15 °C, to relax to the S_1 state. The resulting EPR spectrum was used as a reference and was subtracted from all other spectra to eliminate background contributions due to oxidized cyt b_{559} and impurities. Following the dark adaptation period, samples were illuminated again at −30 °C to obtain the maximum S_2-state population.

EPR measurements were obtained with a Bruker ER-200D-SRC spectrometer interfaced to a personal computer and equipped with an Oxford ESR 900 cryostat, an Anritsu MF76A frequency counter, and a Bruker 035M NMR

Scheme 1: Flow Chart Summarizing the Observations of This and the Accompanying Paper (*26*)[a]

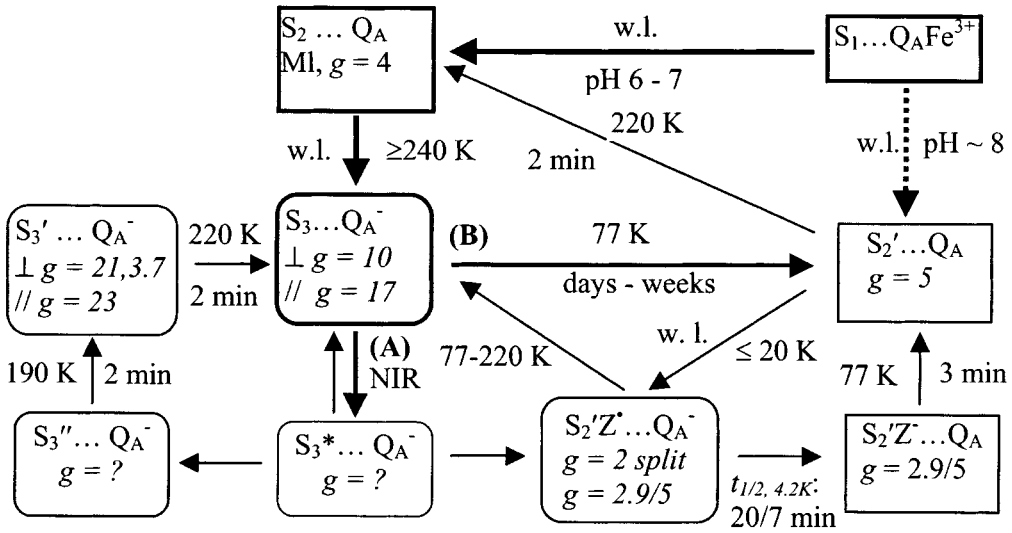

[a] S_3*, S_3'', and S_3' are the NIR excited and transient forms of the S_3 state. S_2' is a modified S_2 state. $S_2'Z^{\bullet}$ and $S_2'Z^-$ are transients involving tyr Z and formed via the indicated pathways, $S_2'Z^{\bullet}$ being assigned to the state giving rise to the split radical signal. The indicated times are those required to complete the corresponding transitions at the respective temperatures. See text for details on the thermal barriers affecting the decay of S_3*...Q_A^- along the two different pathways and on the two half time constants given for the step $S_2'Z^{\bullet}$...Q_A^- to $S_2'Z^-$...Q_A. The dashed arrow represents a tentative pathway at alkaline pH, based on preliminary evidence. Ml represents the Mn-multiline EPR signal. See Materials and Methods for a description of the NIR and white-light (w.l.) illuminations.

gaussmeter. Where not specified, the perpendicular 4102ST cavity was used, and the microwave frequency was 9.39 GHz with 5 mm tubes. The spectra obtained with the standard cavity are the average of 2−4 scans. Tubes of 5 mm were also used with the dual mode cavity, 4116 DM, and 4 or 10 accumulations were done in the perpendicular or the parallel mode, respectively. The microwave frequency was 9.60 GHz in the perpendicular and 9.31 GHz in the parallel mode.

RESULTS

Flowchart. The rather complex phenomenology described in this paper can be rationalized with the help of the flowchart of Scheme 1. Although this chart will be fully justified at the end of the Results section, it is placed here as a guide to tracing the various intermediates.

The scheme starts at the right-upper corner with the state S_1...Q_AFe^{3+}. Illumination of this state at the working pH of 6−7 leads via S_2 to the S_3...Q_A^- state, which is central in Scheme 1. The S_3...Q_A^- state can be converted to various intermediates via two main pathways: (A) excitation by NIR light and (B) slow recombination at 77 K.

Route A, Spectral Changes Induced by Low-Temperature NIR Excitation of the S_3 State. The identified terminal EPR products of the NIR excitation of S_3 are the S_2' ($g = 5$) state and a state characterized by low-field EPR signals at both the perpendicular and the parallel mode (*26*, *42*). This latter state is denoted as S_3' in Scheme 1. The two states evolve along different pathways, as will be justified below, arising presumably from a common precursor state S_3*...Q_A^-, Scheme 1. The decay of S_3*...Q_A^- along the two different pathways is determined by thermal barriers, as will be illustrated below.

De-Excitation of S_3...Q_A^- via Elevated-Temperature Intermediates.* In the experiment of Figure 7 of the accompanying paper, the sample, after NIR excitation at 4.2 K, was kept at the same temperature until the $g \sim 2$ signal decayed almost completely. In a further experiment, Figure 1, the sample, following population of the S_3 state (Figure 1a) and excitation by NIR light for 1 min at 4.2 K, was immediately transferred to 77 K for 5 min.

Figure 1b shows the spectrum recorded following five "NIR at 4.2 K, 5 min at 77 K" cycles. Qualitatively similar spectra were obtained following the first cycle, but the repeated cycles result in an enhanced conversion of the S_3 state. The sample was subsequently transferred to −80 °C for 2 min, Figure 1c, and to −50 °C for 2 min, Figure 1d. The sample was then allowed to relax to the S_1 state, and the spectrum of the S_2 state, showing the yield of this state in this sample, was obtained by illumination at −30 °C, Figure 1e.

The S_3 state is characterized by the broad resonance at $g = 10$ (Figure 1a). At 4.2 K (but not at 11 K), this signal and the signals of the S_2 state ($g = 4.1$ and multiline) are saturated under the present conditions (a detailed account of the temperature and power-saturation dependence of the signals, see also ref. *48*, will be presented elsewhere). In contrast, certain of the signals induced by the NIR excitation are only slightly saturated at 4.2 K, and this allows for a better resolution of the spectral changes at this temperature, as described below.

A $g = 5$ signal is induced in Figure 1b, and this is superimposed on the residual $g = 4.1$ S_2 state signal. The signal is smaller than what would be expected by comparison with Figure 7 of the accompanying paper, particularly if corrected for the contribution of the S_2 $g = 4.1$ signal (see Materials and Methods). A more accurate comparison will be made with the experiment of Figure 3 that is described below. Pronounced changes occur following 2 min incubation at −80 °C (Figure 1c). The $g = 5$ signal decreases, and new signals appear at $g = 21$ and 3.7. The $g = 21$ signal was presented in the previous study, but the $g = 3.7$ derivative-shaped contribution was not specifically mentioned, although it was apparent in the spectra (*42*). It was observed that the

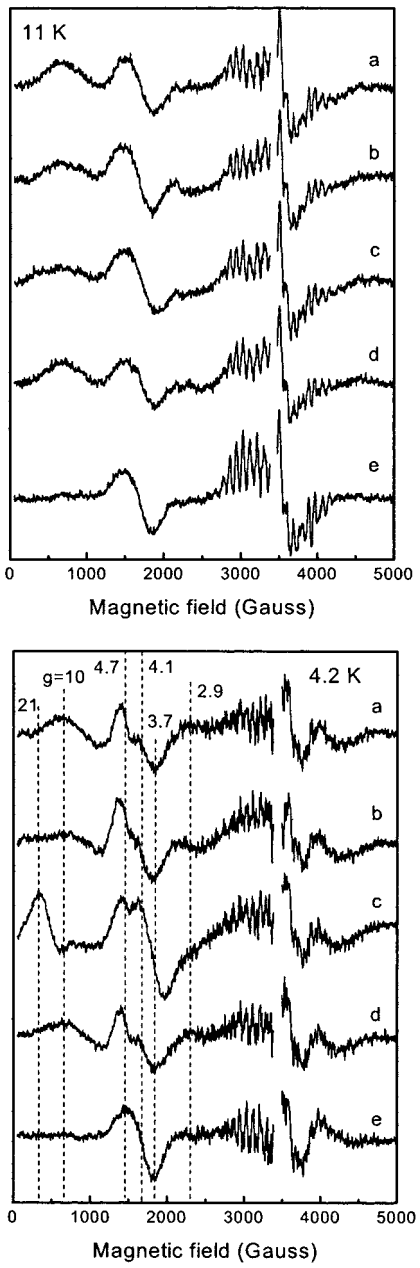

FIGURE 1: Conversion of the S_3 state by NIR excitation at 4.2 K followed by immediate transfer to 77 K and then annealing at higher temperatures. (a) S_3 state as prepared. (b) Following five subsequent cycles of NIR illumination for 1 min at 4.2 K immediately followed by transfer at 77 K for 5 min. (c) Subsequent incubation at − 80 °C for 2 min. (d) Subsequent incubation at − 50 °C for 2 min. (e) The sample was subsequently allowed to relax to the S_1 state at 4 °C, and the spectrum of the S_2 state was obtained by illumination at −30 °C. All spectra are difference spectra obtained after subtraction of the dark-adapted (S_1) spectrum as described in the Materials and Methods section. EPR conditions: recording temperatures 11 and 4.2 K (same plotting scale), bimodal cavity, receiver gain 6300, microwave frequency 9.60 GHz, microwave power 32 mW, modulation amplitude 10 Gpp, modulation frequency 100 kHz.

$g = 21$ and 3.7 signals appear with constant relative ratio in all our experiments. It will be therefore tentatively assumed that they belong to the same electronic configuration. The state represented by the $g = 21/3.7$ signals, and their parallel mode counterparts (to be described below) will be referred to as an S_3' state.

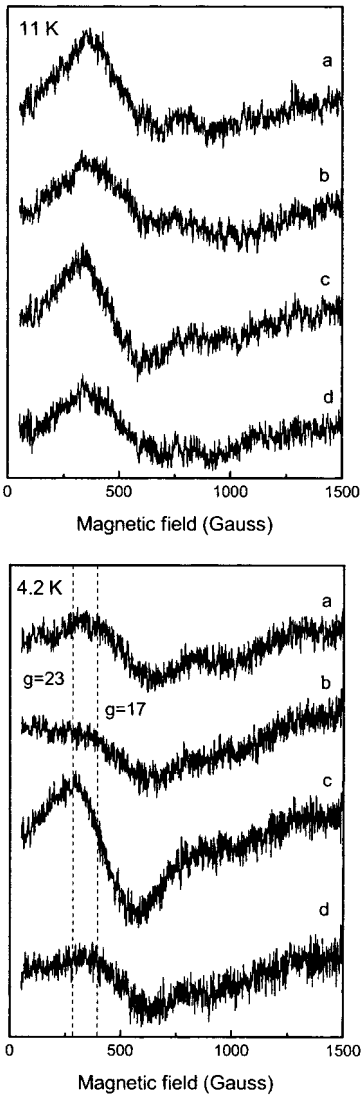

FIGURE 2: Effects of the NIR illumination on the S_3-state parallel-mode spectra, recorded at 11 and 4.2 K (same plotting scale). Labeling of the spectra is the same as that in Figure 1a−d. EPR conditions: receiver gain 63000, microwave frequency 9.31 GHz, microwave power 126 mW (spectra at 11 K), 8 mW (spectra at 4.2 K) modulation amplitude 10 Gpp, modulation frequency 100 kHz.

All signals induced by the above procedure disappear, and the $g = 10$ signal is restored to about 75−80% of its initial intensity, following 2 min incubation at −50 °C (Figure 1d). The enhancement of the untreated S_3-state spectrum at $g = 10$ appears to occur at the expense of the $g = 21/3.7$ (S_3') EPR signals. Another observation, to be contrasted later with the experiment of Figure 3, is that after the incubation at −50 °C (Figure 1d, 11 K) the multiline signal is not significantly enhanced, at least to a detectable level, in comparison to its initial intensity (Figure 1a).

The events depicted in Figure 1 were also followed using parallel mode EPR, and this is shown in Figure 2 (where the labeling of Figure 1 is preserved). Figure 2a shows the spectrum of the S_3 state as prepared. The broad characteristic signal at low fields ($g \sim 17$) (*42*) is clearly visible. The spectrum at 4.2 K appears weaker because lower microwave power has been used to reduce saturation. Following the NIR-illumination-at-4.2 K 5 min-at-77 K cycles, the $g \sim 17$ peak is greatly diminished, Figure 2b, matching the diminution

of the $g = 10$ signal in perpendicular mode (Figure 1). Drastic changes occur upon subsequent incubation at −80 °C for 2 min (Figure 1c). A new feature at $g \sim 23$ appears. Notable is the relatively large intensity of the signal at 4.2 K. Preliminary experiments show that this signal, unlike the $g \sim 17$, does not saturate easily at 4.2 K. A detailed study of the saturation properties of the various signals is currently in progress. At 11 K, Figure 2c, the signal is a mixture of the $g = 23$ and a portion of the initial $g = 17$ signal, which does not saturate at this temperature. Further warming to −50 °C for 2 min restores by about 80% the spectral feature of the initial S_3 state (Figure 2d), in agreement with the spectra at perpendicular mode. It should be noted, however, that the determination of signal intensities at parallel mode is hampered by uncertainties in the baseline.

The behavior of the parallel-mode spectra in Figure 2 closely follows the observed changes in their perpendicular mode counterparts, Figure 1. It appears therefore that the $g \sim 23$ signal (Figure 2c) accompanies the $g = 21/3.7$ signals at perpendicular mode EPR (Figure 1c), S_3' state, just as the $g \sim 17$ (parallel) accompanies the $g \sim 10$ (perpendicular) in the untreated S_3 state (*48, 42*).

Decay of S_3...Q_A^- at Liquid Helium Temperatures.* The intermediates of the S_3*...Q_A^- decay at 4.2 K were examined in the experiment of Figure 7 of the preceding paper (*26*). These include the metallo−radical state $S_2'Z^{\bullet}...Q_A^-$, the transient charge-recombination product at 4.2 K $S_2'Z^-...Q_A$, and the terminal $S_2'...Q_A$ state, Scheme 1. Figure 3 is an extension of the experiment of Figure 7 of the accompanying paper (*26*) and is included here for comparison with the decay products of $S_3...Q_A^-$ at elevated temperatures in Figure 1.

Following production of the S_3 state, Figure 3a, four cycles of NIR-excitation and dark adaptation (for 40 min) at 4.2 K were performed to enhance the NIR induced changes. The spectral changes during the NIR excitation and decay at 4.2 K are not repeated here, as they were adequately described in Figure 7 of the preceding paper. At the end of the fourth cycle, the sample was transferred to successively higher temperatures: 77 K for 5 min, Figure 3b, −80 °C for 2 min, Figure 3c, and −50 °C for 2 min, Figure 3d. The sample was allowed to relax to the S_1 state at the end, and the spectrum of the S_2 state obtained by illumination at −30 °C was recorded, Figure 3 e.

The trend in the spectra of Figure 3 is qualitatively similar to the changes observed in Figure 1. Important quantitative differences can be noted, however. The $g = 5$ signal in Figure 3b is larger than the corresponding signal in Figure 1b, particularly if one takes into account the interference from the $g = 4.1$ signal of the S_2 state (see Materials and Methods). On the contrary, the $g = 21/3.7$ signal, formed by subsequent incubation at −80 °C (Figure 3c), is smaller relative to its counterpart in Figure 1c. These differences are not large, but they are reproduced in all similar experiments. It appears therefore that incubation of the NIR excited state at liquid helium temperatures favors the S_3*...Q_A^- to $S_2'...Q_A$ branch, while higher temperatures favor the transition to the S_3' intermediate.

In support of the above observations, noticeable in Figure 3 (spectra at 11 K) is an increase (by 20−25%) in the S_2-state spectral intensities following the −50 °C incubation step (Figure 3d) as compared to their initial levels in Figure 3a. Assuming, approximately, equal initial populations of

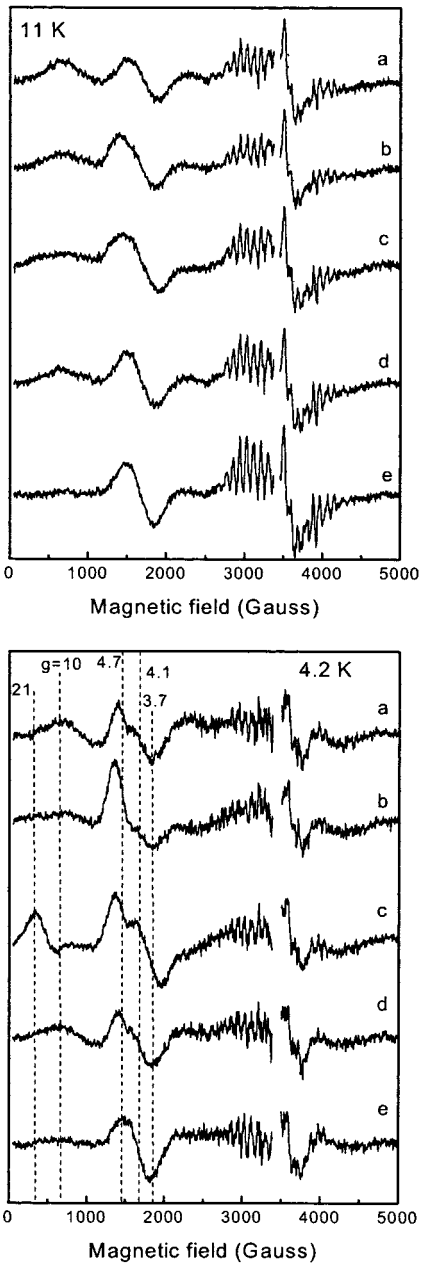

FIGURE 3: Conversion of the S_3 state, following NIR excitation at 4.2 K and dark adaptation at 4.2 K, and then annealing at higher temperatures. (a) The S_3 state as prepared. The sample was subsequently subjected to four cycles of NIR-light excitation and subsequent 40 min dark adaptation at 4.2 K and successively incubated (b) at 77 K for 5 min, (c) at −80 °C for 2 min, and (d) at − 50 °C for 2 min. (e) The sample was subsequently allowed to relax to the S_1 state at 4 °C, and the spectrum of the S_2 state was obtained by illumination at −30 °C. All spectra are difference spectra obtained after subtraction of the dark-adapted (S_1) spectrum as described in the Materials and Methods section. EPR conditions: Spectra were recorded at 11 and 4.2 K (same plotting scale), with a bimodal cavity, receiver gain 6300, microwave frequency 9.60 GHz, microwave power 32 mW, modulation amplitude 10 Gpp, and modulation frequency 100 kHz.

the S_2 and S_3 states (see Materials and Methods), it appears that the missing population of S_3 has decayed to S_2. As the decay of the S_3 state at −50 °C is slow (*26*), the major portion of the S_3-to-S_2 conversion must be attributed to the NIR-induced charge recombination via the $S_2'(g = 5)$ intermediate. The above changes should be accompanied by a decline in the $Q_A^-Fe^{2+}$ signal. As, however, this signal in

Figure 1a represents 100% of the centers and is inherently weak, the expected decrease of 10−12% would be difficult to detect. Careful comparison of the spectra indicates that the final intensity of the iron−semiquinone (Q_A^-Fe(II)) signal shown in Figure 3d appears indeed diminished in comparison to that of the initial S_3 state, but it is difficult to determine the step at which the major decrease occurs. Figure 3e is included as a reference and shows the spectrum of the S_2 state.

The Two Pathways of Decay of the NIR-Excited S_3 State Leading to the $S_3'(g = 21/3.7)$ and $S_2'(g = 5)$ Intermediates Are Separate. The $g = 21/3.7$ conformation in the spectra of Figure 1 does not form at the expense of the $g = 5$ signal. The $g = 5$ state is a half-integer-spin state, $S = {}^7/_2$ (odd number of unpaired electrons) (*45*), assigned to a lower oxidation state of the OEC, S_2' (*26*, *41*). The $g = 21/3.7$ configuration having parallel mode components is assigned to a state with an even number of unpaired electrons (a modified S_3, S_3'). Furthermore, no correlation could be found between the $g = 5$ and 21/3.7 signal sizes. More notably, in the following experiments relating to route B of Scheme 1 (Figures 4−6 below), a sample with a prominent $g = 5$ signal (S_2' state) leads by illumination to the $S_2'Z^{\bullet}...Q_A^-$ intermediate (Scheme 1), but clearly no $g = 21/3.7$ signal is formed after annealing to −80 °C. Therefore, the S_3' and S_2' pathways evolve independently and branch earlier than the metallo−radical intermediate $S_2'Z^{\bullet}...Q_A^-$. A common precursor state, S_3*, is assumed. The pathway of S_3* to S_3' is assumed to proceed via an unidentified intermediate, denoted as $S_3''...Q_A^-$ in Scheme 1. S_3'' appears to be an EPR-silent configuration and is introduced to account for the absence of a detectable predecessor of the $g = 21/3.7$ configuration during the 77 K incubation step, Figures 1b and 3b. At 4.2 K (but not at 77 K), the transition of S_3* to S_3'' occurs more slowly than the evolution of the metallo−radical intermediate. This is suggested by the reduced formation of the $g = 21/3.7$ configuration in the experiment of Figure 3. The transition of S_3'' to S_3' requires higher temperatures for activation, a few min at 200 K. It is interesting, however, that this latter transition can be activated by prolonged NIR illumination at 4.2 K: in other experiments (not shown) where S_3'' was reached by NIR illumination of S_3 at 4.2 K and incubation (a few min) at 77 K, subsequent prolonged NIR illumination at 4.2 K resulted in the evolution of a significant fraction of S_3' ($g = 21/3.7$ signal) during a few minutes of dark adaptation at 77 K.

Route B. Prolonged Storage of the S_3 State at 77 K and Subsequent Light Excitation. It was shown in the accompanying paper that prolonged storage of S_3 state samples at 77 K results in the conversion of the $g = 10$ signal to $g = 5$. The latter was assigned to an excited S_2 state configuration, S_2', with spin $S = {}^7/_2$ (*45*). Nugent et al. (*41*) showed that light excitation of this state at liquid-helium temperatures induces a $g \sim 2$ broad radical signal. This signal appears to be similar to the $g \sim 2$ signal induced by NIR excitation of the S_3 state (*42*). The phenomenology accompanying the $g \sim 2$ signal formation in Nugent et al. (*41*) is interesting, and we have looked at the respective changes more closely.

Figure 4 shows the effect of white-light illumination of samples prepared in the S_3 state and subsequently incubated at 77 K for 2 months. The initial S_3 state is shown in Figure 4a. Following 2 months storage at 77 K, the S_3 state $g = 10$ signal decreased significantly, and the sample developed a strong $g = 5$ signal (Figure 4b). At the same time, the Q_A^-Fe(II) signal decreased to about 30% of its initial size, due to charge recombination. The recombining partners in this particular experiment were approximately estimated to be S_3 in 24% of the centers, S_2 in 9%, and tyr $D^{\bullet}$ in 37%. The estimations were based on a comparison of the initial and final signal levels, as was described in the experiment of Figure 3 of the preceding paper (*26*). The sample was subsequently illuminated at 4.2 K with a white-light source

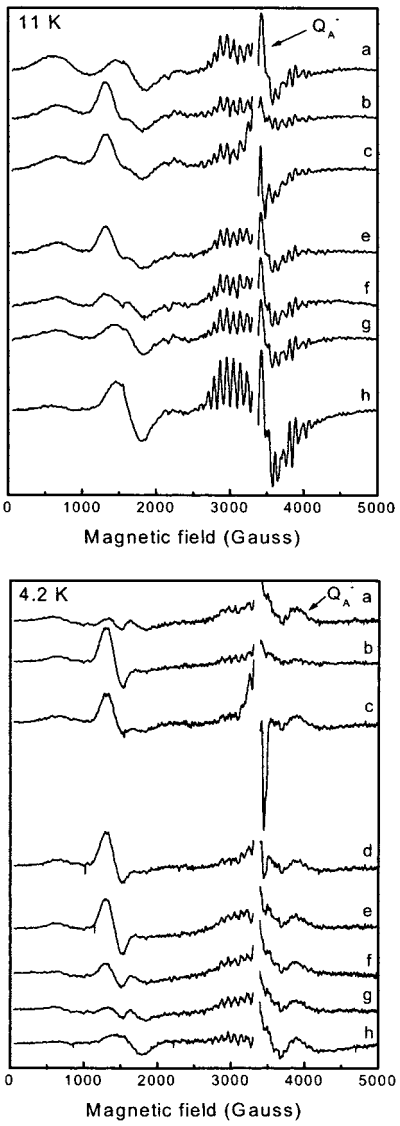

FIGURE 4: Prolonged incubation of the S_3 state at 77 K and the effect of visible-light excitation at 4.2 K. The same sample was treated successively as follows: (a) S_3 state as prepared, (b) incubation at 77 K for 55 days, (c) illumination with visible light for 1 min at 4.2 K, (d) incubation at 4.2 K for 30 min and at 11 K for 30 min, (e) incubation at 77 K for 10 min, (f) incubation at −80 °C for 3 min, and (g) incubation at − 50 °C for 2 min. (h) The sample was subsequently allowed to relax to the S_1 state at 4 °C and the spectrum of the S_2 state was obtained by illumination at −30 °C. All spectra are difference spectra obtained after subtraction of the dark-adapted spectrum as described in the Materials and Methods section. The spectra at 4.2 K are scaled down by a factor of 2 relative to the 11 K spectra. EPR conditions: standard cavity, receiver gain 6300, microwave frequency 9.39 GHz, microwave power 32 mW, modulation amplitude 25 Gpp, modulation frequency 100 kHz.

(Figure 4c). A $g \sim 2$ signal developed with a concomitant decrease of the $g = 5$ signal (see also *41* and Figure 6). Notable is also the restoration to ~85% of the Q_A^-Fe(II) signal, indicating the rereduction of ~55% out of the 70% centers that had recombined during the 2-month storage. This was accompanied by an approximate restoration of the signal II size (i.e., oxidation of tyr D in a maximum of 35% of the centers). As no other donor appeared to be oxidized, we suggest that the species represented by the $g \sim 2$ radical is the alternative electron donor.

Following 60 min storage at 4.2−11 K, the radical signal decayed to a very small level, while the initial intensity of the $g = 5$ signal was restored partially (Figure 4d), and the Q_A^-Fe(II) signal decreased to ~75% (and remained at this level in the following spectra). The decay of the $g \sim 2$ signal is attributed to charge recombination of this species with the Q_A^-Fe(II) species and in part to oxidation of the Mn cluster (see below). A subsequent storage for 10 min at 77 K (Figure 4e) resulted in an additional increase of the $g = 5$ intensity to about 90% of its initial size. Brief incubation at −80 °C (Figure 4f) resulted in a significant decrease of the $g = 5$ signal, but unlike the experiments of Figures 1 and 3 with the NIR excitation of the S_3 state, no $g = 21/3.8$ signal developed. This observation supports strongly the independence of the two pathways branching out of the NIR-excitation of the S_3 state (see previous section).

Effects similar to those in Figure 4 are also observed by NIR instead of visible light excitation of samples that had been stored at 77 K. The results in this case are, however, complicated by the changes induced to the remaining native S_3 state. The NIR excitation of the portion of centers that have not decayed during prolonged incubation at 77 K, and thus are still at the S_3 state, results in spectral changes similar to those reported in Figures 1 and 3.

Transition of S_2' to S_2 at Elevated Temperatures. Starting at −80 °C but more notably at −50 °C (Figure 4g), the relaxation of the $g = 5$ and partial decay of the remaining $g = 10$ signal resulted in an increase of the S_2 multiline, as compared to the spectrum in Figure 4b (11 K). The conversion of the $g = 5$ (S_2' state) to the multiline and $g = 4.1$ signals (S_2 state) at elevated temperatures was noted earlier (*41*) and also in the preceding paper (*26*) and in Figure 3 of the present paper and is accounted for by the S_2' to S_2 branch in Scheme 1.

White-Light Excitation of the S_2'...Q_A State Produces the Same Metallo−Radical Intermediate, $S_2'Z^{\bullet}$...Q_A^-, That is Reached by NIR-Light Excitation of the S_3 State. (a) Comparison of the $g \sim 2$ Signals and Decay Kinetics. In Figure 5, we compare the $g \sim 2$ signal of a fresh S_3 sample excited by NIR light (Figure 5a) to the spectrum of a 77 K stored sample excited by visible light (Figure 5b). The spectra within the present experimental resolution appear very similar.

However, a notable difference exists in the decay kinetics of the two signals. The inset in Figure 5 shows two typical decay-kinetic traces of the $g \sim 2$ signal induced in a fresh S_3 sample and in a 77 K stored S_3 sample, at 4.2 K. The decay curves are best fitted with two exponential components. Thus, in the case of the fresh sample, the signal decays with half times of approximately 20 and 185 min, while in the 77 K stored sample the half times decrease to approximately 7 and 35 min. This difference is unexpected

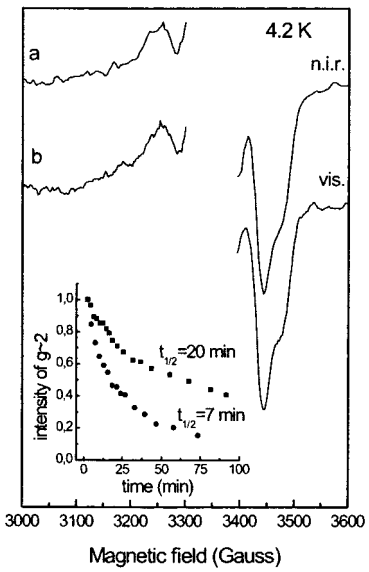

FIGURE 5: Broad radical at $g \sim 2$ in freshly prepared and 77 K stored S_3 state samples. (a) Freshly prepared S_3 sample; induction by NIR illumination. (b) S_3 sample incubated at 77 K for 55 days, visible-light induction. In both cases, the spectrum prior to illumination at 4.2 K has been subtracted. EPR conditions: receiver gain 6300, microwave frequency 9.39 GHz, microwave power 32 mW, modulation amplitude 25 Gpp, modulation frequency 100 kHz. Inset: comparison of the decay rates of the broad radical in the two cases. Squares, freshly prepared sample. Circles, sample incubated at 77 K for 55 days.

since both $g \sim 2$ signals appear to be identical and their decay at 4.2 K is attributed to charge recombination with Q_A^-. It may be argued that the difference lies in the Q_A^- acceptor. In fresh samples, Q_A^- is trapped by the initial illumination leading to formation of S_3. In the 77 K stored samples, Q_A^- is reformed by illumination at 4.2 K after its slow oxidation at 77 K. Therefore, there could be conformational differences at the acceptor side according to which the Q_A^- radical is more stable when formed at −30 °C, rather than when formed at 4.2 K. An alternative explanation is, however, the following. The formation (via the NIR-excited S_3* intermediate) and decay (via recombination with Q_A^-) of the $g \sim 2$ radical in the fresh samples may have comparable time constants, resulting in an apparent slow decay of the radical. In comparison, the formation of the $g \sim 2$ radical in 77 K stored samples (S_2' state), via oxidation by P_{680}^+, must be very fast.

To account for the above observations, two half times are indicated in Scheme 1 for the step $S_2'Z^{\bullet}$...Q_A^- to $S_2'Z^-$...Q_A. The longer probably contains contributions from the step S_3* to $S_2'Z^{\bullet}$, while the shorter is probably the true one and is measured during the cycle S_2'...Q_A to $S_2'Z^{\bullet}$...Q_A^- to $S_2'Z^-$...Q_A.

(b) Changes in the $g \sim 5$ Signal. As was noted in Figure 4, white-light excitation of S_3 samples that decayed to the S_2' state by prolonged storage at 77 K results in the formation of the $g \sim 2$ signal concomitantly to the decrease of the $g = 5$ signal (see also *41*). The diminution of the latter signal is more clearly shown in the difference spectra of Figure 6.

Spectrum a is the difference of spectrum c − spectrum b in Figure 4 at 4.2 K, while spectrum b is the same difference at 11 K. It is apparent that white-light irradiation also results in the appearance of the $g = 2.9$ derivative signal. This can be explained in the context of the analysis of the $g = 5/2.9$ signals employing an $S = {}^7/_2$ spin Hamiltonian (*26*, *45*).

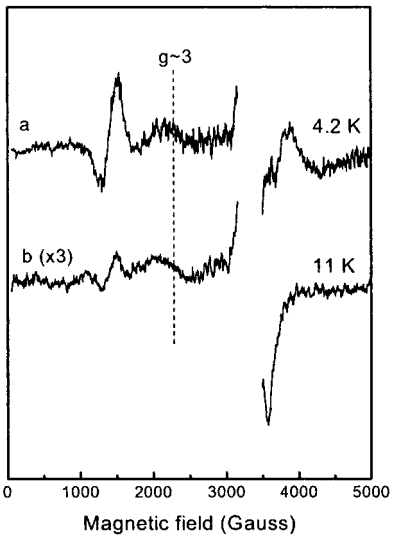

FIGURE 6: Induction of the $g = 2.9$ signal and decrease in the $g = 5$ component caused by visible-light illumination at 4.2 K of a 77 K stored S_3 sample. (a) Difference spectrum generated by subtraction of spectrum b from c of Figure 4, at 4.2 K. (b) The same difference but at 11 K. EPR conditions are the same as those in Figure 4.

Small changes in the crystal field parameters would cause a deviation from the symmetry that favors a nearly isotropic $g = 5$ signal and induce a diminution and perhaps broadening of the $g = 5$ feature and the appearance of the $g = 2.9$ contribution. As the exciting light may not be fully efficient in converting all centers, the spectrum in Figure 4c is probably a mixture of the unperturbed and the modified configuration.

It appears that the above crystal field change is triggered by the formation of the $g \sim 2$ broad radical. The $g = 5$ signal recovers slowly at 4.2 K during the decay of the $g \sim 2$ signal, Figure 4d. Analysis of kinetic traces (not shown) indicates that the $g = 5$ recovery is biphasic with $t_{1/2} \sim 20$ min for the first phase. The second component is very slow and difficult to determine with accuracy (half time in the range of hours). Thus, the recovery rate of the $g = 5$ signal is slower than the decay rate of the broad radical at $g \sim 2$. In the paper of Nugent et al. (*41*), it was assumed that the two kinetic traces were similar, but careful examination of their data shows a faster decay of the $g \sim 2$ signal. The latter decays via recombination with the acceptor side as discussed above, while the $g = 5$ species requires warming up to 77 K in order to reorganize and regain its initial crystal field parameters (*26*, *45*). The situation is fully analogous to the evolution of the $g \sim 2$ and $g = 5/2.9$ signals following NIR excitation of the S_3 state described in the experiment of Figure 7 of the accompanying paper.

The $S_2'Z^{\bullet}...Q_A^-$ to $S_2'Z^-...Q_A$ to $S_2'...Q_A$ pathway in Scheme 1 describes, accordingly, the gradual conversion of the metallo−radical intermediate regardless of how this state was reached. The metallo−radical state, $S_2'Z^{\bullet}...Q_A^-$, has also an alternative pathway of de-excitation as discussed below.

The Metallo−Radical Intermediate $S_2'Z^{\bullet}...Q_A^-$ Converts to $S_3...Q_A^-$ at Elevated Temperatures. In the experiment of Figure 4, the sample, following light excitation at 4.2 K, was incubated at the same temperature until the broad radical decayed. This resulted in charge recombination between the radical species and $Q_A^-Fe^{2+}$, as judged by the decrease of the $Q_A^-Fe^{2+}$ signal. In the experiment of Figure 6 of the companion paper (*26*), the sample was transferred to temperatures higher than 77 K immediately after the light excitation at 4.2 K. Charge recombination was negligible in this case, and an enhancement of the S_3 signal at $g = 10$ was observed instead. It appears accordingly that storage at 4.2 K favors recombination of Q_A^- with the radical, while at 77 K and above the positive hole on the radical is probably transferred further on the donor side and charge separation is stabilized (*41*). It is interesting that a similar phenomenology applies to what appears to be an $S_1Z^{\bullet}$ state produced recently by white-light excitation of S_1 at liquid-helium temperatures (*49* see also *20*). It would be more difficult to confirm this high-temperature pathway with samples prepared in the $S_2'Z^{\bullet}...Q_A^-$ state by NIR excitation of S_3, due to the presence of a significant fraction of centers that convert to S_3 via the S_3' pathway. Given the similarity of the $S_2'Z^{\bullet}...Q_A^-$ states regardless of the way they were reached, we assume in Scheme 1 that the high-temperature conversion to S_3 is a common property of this metallo−radical intermediate.

S_1 Advances to S_2' at Alkaline pH. It was shown in the accompanying paper that illumination at −30 °C of samples prepared in the S_1 state at pH 8.1 produces the $g = 5$ signal, characteristic of the S_2' state. It appears accordingly that the S_2' state, while being a transient state at pH 6.5 (trapped at 77 K), is comparatively stable at alkaline pH and can be formed directly by illumination of the S_1 state at elevated temperatures. Until the pH effects are more systematically studied, the S_1-to-S_2' transition at high pH will be considered as tentative and is shown with a dashed arrow in Scheme 1.

DISCUSSION

The Split Radical Signals at $g = 2$ Are Assigned to Tyr $Z^{\bullet}$. Very similar (probably identical) $g = 2$ signals are induced by two different mechanisms. In S_3 samples that have decayed by charge recombination at 77 K (and have thus reached the state $S_2'...Q_A$), production of the $g \sim 2$ signal is due to light-induced charge separation (see also Nugent et al., *41*). In fresh S_3 samples, induction of the $g = 2$ signal clearly is not due to charge separation, since the primary acceptor, $Q_A^-Fe(II)$, is reduced in all centers prior to the low-temperature excitation. Besides, the effect is favored at NIR wavelengths that are not efficient in producing charge separation. Formation of the signal in this case parallels changes in the S_3 EPR signals, suggesting that the signal is the result of internal rearrangements in the Mn cluster (*42*, see also below). The decay of the split radical signals at 4.2 K is attributed to charge recombination with Q_A^-, while at elevated temperatures, transfer of the positive hole to the Mn cluster is favored. These properties suggest a common origin of the $g = 2$ signals in the two cases. The radical responsible for the signal is clearly a donor in redox equilibrium with the Mn cluster, located close enough to the cluster, so that it is broadened by magnetic interaction with the Mn and can have an electrostatic influence on the crystal-field at the Mn site (*26*). The signal is reminiscent of the broadened radical observed in inhibited samples and assigned to tyr $Z^{\bullet}$ interacting with the S_2 state of the cluster (*10*, *32*−*36*). It is reasonable to assign the radical signal to tyr $Z^{\bullet}$ as well.

Flowchart of the Various Events. The complex phenomenology described in this and the companion paper can be

followed more easily by means of the flowchart depicted in Scheme 1. Following formation of the S_3 state by white-light excitation of the S_2 state, two main routes are indicated as described below.

Route A: Immediate excitation by NIR light at temperatures below about 77 K results presumably in the formation of an excited S_3 state, denoted S_3*. S_3* decays to various intermediates via either of two pathways. Slowly at liquid helium temperatures but much faster at 77 K, S_3* decays to an undefined state, denoted S_3'', which by raising the temperature to ca. 190 K decays to a spin state characterized by signals at $g = 21$, 3.7 in perpendicular mode, and 23 in parallel mode, denoted S_3'. Upon further warming to 220 K, S_3' relaxes to the untreated S_3 state. Of particular interest is the alternative pathway via the intermediate $S_2'Z^{\bullet}...Q_A^-$. This metallo−radical transient can be trapped below about 77 K (more favorably at liquid helium temperatures) and is characterized by the split radical $g = 2$ signal and the $g = 5/2.9$ configuration of the Mn cluster. At elevated temperatures tyr $Z^{\bullet}$ reoxidizes S_2' to the initial S_3 state. At temperatures below about 20 K, tyr $Z^{\bullet}$ recombines with Q_A^-, leaving the cluster in the $S_2'Z^-$ state. This latter state may be differentiated by the same state in the presence of tyr $Z^{\bullet}$ by a somewhat more intense $g = 5$ signal. This could result from a small change in the crystal field parameters. Further warming to 77 K induces a change in the crystal field parameters of this configuration, which results in the narrowing and increase of the $g = 5$ signal and the loss of the $g = 2.9$ signal (S_2' state) (*26*, *45*).

Route B: Upon prolonged incubation at 77 K, the S_3 state recombines slowly with Q_A^- to yield a modified S_2 state (S_2', $g = 5$) presumably identical to the respective state above. The S_2' state relaxes to the untreated S_2 state at significantly higher temperatures, 220 K. Light excitation of the S_2' state at liquid-helium temperatures results in charge separation and trapping of the metallo−radical intermediate $S_2'Z^{\bullet}...Q_A^-$ characterized by the split $g = 2$ signal, loss of $g = 5$ intensity, and the appearance of the $g = 2.9$ feature. The properties of this state are similar to the respective state reached via route A, except that the recombination rate between tyr $Z^{\bullet}$ and Q_A^- is 3 times faster. As was discussed in relation to the data of Figure 5 of the present paper, the difference may lie on the acceptor side or on the interference of the rate of formation of $S_2'Z^{\bullet}$ from the precursor state S_3* when reaching the metallo−radical intermediate via route (A).

It is interesting that the terminal state of both routes, S_2', can be reached by direct light excitation of S_1 at alkaline pH. This not only confirms the assignment of the $g = 5$ signal to an S_2 configuration but also supports the suggestion that S_2' is a proton deficient configuration.

Insights into the Molecular Mechanism. The changes occurring during the various steps in Scheme 1 can be rationalized with the help of a simple molecular model to be described below. The model borrows ideas from the elaborate theoretical study of Siegbahn (*16*), but it is simplified and stripped down to the constituents that are essential for understanding the present results. The main assumptions in constructing the model are the following:

(i) A Mn(III) is present in the S_3 state. This is supported by the sensitivity of S_3 to NIR excitation. This sensitivity was observed first in the S_2 state and was attributed to excitation of a Mn(III) ion (*43*, *44*, *50*), although this is not proven at present. The presence of a Mn(III) ion in the S_3 state would suggest that no Mn oxidation occurs during the S_2-to-S_3 transition in models assuming a $Mn(III)Mn(IV)_3$ valence composition of the S_2 state (favored by most groups (see, e.g., refs *23*, *51*), but see ref *24* for an alternative, $Mn(III)_3Mn(IV)$, view.

(ii) We favor the presence of a radical in the S_3 state. This does not follow directly from the EPR spectra of the unperturbed S_3 state (*48*, *42*) (a radical strongly coupled to the Mn should lead to integer spin states just like, e.g., a $Mn(IV)_4$ configuration) or from the results presented in this paper (it is not essential either for understanding the present phenomenology). It is suggested, however, by a number of observations. Recent Mn Kβ X-ray emission spectroscopy (*23*) added strong weight to the interpretation of XANES results assuming ligand-centered oxidation (*52*), as opposed to Mn oxidation (*53*, *54*) during the S_2-to-S_3 transition. Independent support for the presence of a radical in the S_3 state is provided by the unusual reactivity of NO with the S_3 state and the known preference of NO for certain radicals. Fluorescence experiments at ambient temperatures indicate that NO reduces S_3 to S_1 5 times faster than S_2 to S_1 (*55*). This trend is opposite to what is observed with hydrazine or hydroxylamine (*56*; Schansker, G. and Petrouleas, V. Manuscript in preparation), and the results can be best explained if we assume that the radical is in a bridging position (*6*, *16*, *23*).

(iii) Tyr Z is placed approximately at the third coordination sphere of Mn. This is compatible with the observed relatively weak magnetic coupling of tyr $Z^{\bullet}$ with the spin of Mn both in inhibited (*37*−*40*) and untreated preparations ($g \sim 2$ signal in the present case), as well as with the current crystallographic data, suggesting a 7 Å closest distance between tyrosine and the Mn (*25*). A water molecule is suggested to bridge the Mn ligands and the tyrosine. Future refinements could consider the presence of calcium at this site.

(iv) Insights into the protonation state of tyr Z. There is general agreement that tyr Z in the oxidized state is neutral (deprotonated) (for reviews, see, e.g., refs *1*, *3*, *5*, *57*, *58*, *59*). The protonation state when the tyrosine is reduced is less obvious. A protonated neutral tyrosine is often assumed particularly in models suggesting a proton (or hydrogen atom) abstraction role of this tyrosine (*10* − *12*). Alternatively, certain groups favor a deprotonated-reduced tyrosine (*13*, *20*, *57*, *60*). The question on the protonation state of tyr Z relates to the issue of the proton contacts of tyr Z with its environment, a complex issue by itself, complicated even further by the fact that most of the available studies are on Mn depleted or inhibited preparations (for detailed recent reviews, see refs *58* and *61*). Independent evidence on this important issue can be obtained by comparison of the low-temperature electron donating properties of tyr Z with the better-understood tyr D.

Tyr D is neutral in both the reduced and the oxidized state (reviewed in *58*). Reduced tyr D cannot displace its proton at cryogenic temperatures and therefore cannot be oxidized by P_{680}^+ (the oxidation potential of the $D(H)/D(H)^+$ couple is prohibitively high (*58*)). Tyr D is a good electron donor only at temperatures above about 200 K where the proton can leave. However, oxidized tyr D can be slowly reduced by recombination with Q_A^- at 77 K, giving presumably the

Scheme 2: Molecular Model of the Sequence of Events Described in Scheme 1[a]

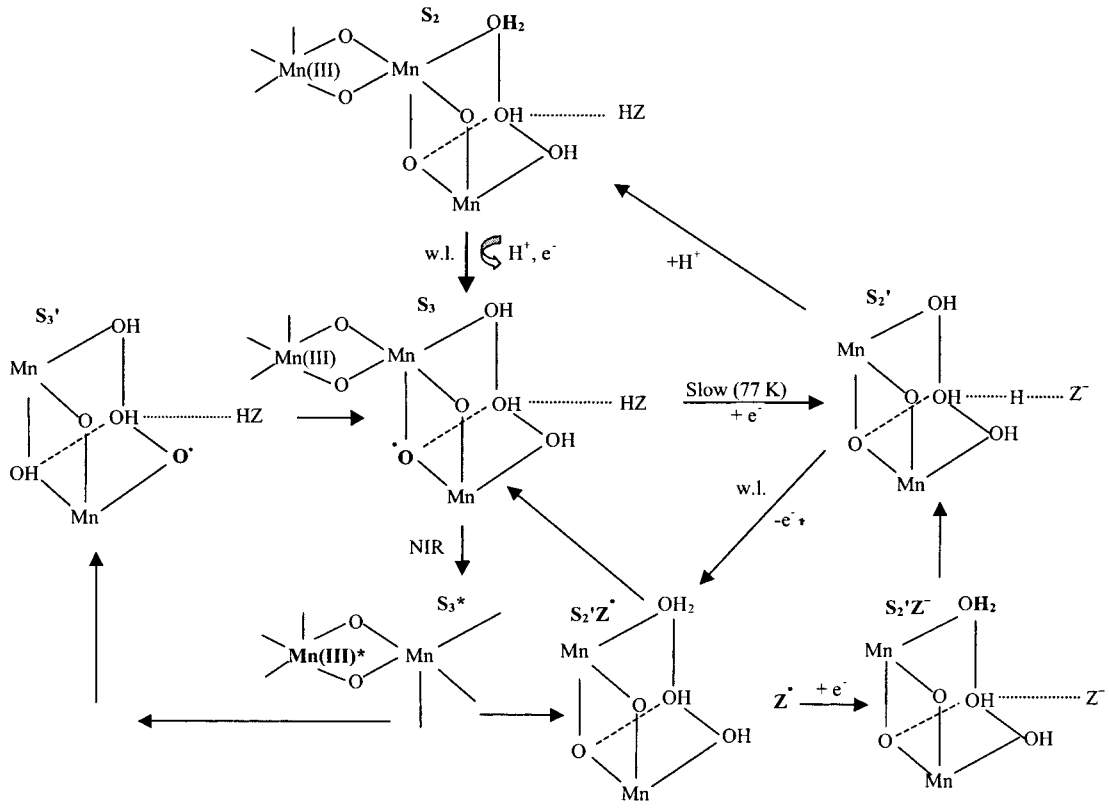

[a] Atoms where the primary changes occur during each transition are drawn in bold. Nonessential atoms (a fourth Mn, Ca^{2+}, Cl^{-}) are omitted, and certain intermediates have been simplified for clarity.

reduced-deprotonated tyrosine. In this state, tyr D^{-} is a very efficient electron donor even at 4.2 K (reviewed in *62*; see also preceding paper, *26*).

Tyr Z exhibits a behavior analogous to that of tyr D in preparations were the Mn cluster is removed or inhibited by a number of treatments (*32*). We suggest that the reduced tyr Z in these inhibited preparations is protonated at ambient temperatures, and the proton abstraction pathway is inefficient at low temperatures. The presence of the native Mn cluster appears to improve the low-temperature electron-donating efficiency of tyr Z. In untreated preparations, the S_1-to-S_2 transition is known to efficiently occur at temperatures close to 77 K. Furthermore, recently Nugent et al. (*49*; see also ref *20*) provided evidence that illumination of the S_1 state at 4.2 K produces the intermediate $S_1Z^{\bullet}$, which upon subsequent annealing to 77 K advances to the S_2 state. Interestingly, the same intermediate is produced by NIR excitation of the S_2 state at 4.2 K (Koulougliotis and Petrouleas unpublished). Additional evidence is provided by the present experiments. White-light excitation of the transient state S_2' or NIR excitation of S_3 at liquid helium temperatures invariably produces the same spectrum attributed to a broadened tyr $Z^{\bullet}$ signal (see also below). A common observation in control experiments during the present studies is, however, that no tyr $Z^{\bullet}$ signal could be induced by visible-light illumination at 4.2 K of the untreated S_2 state (see also ref *41*). A similar observation was also made in the state $S_3...Q_A$, trapped by illumination/dark-adaptation cycles in the presence of an exogenous quinone (results not shown). This indicates a more efficient deprotonation of tyr Z at 4.2 K in the lower S-states unless a higher S state is already de-protonated, like S_2'.

It is apparent from the above that the question on the protonation state of reduced tyr Z may not have a unique answer. The strength of the hydrogen bonding in the native OEC may depend on the S state, and the extent of deprotonation of the Mn cluster, due to environmental factors, e.g., the pH. The situation with the oxidation of tyr Z by low-temperature charge separation (this brings an extra positive charge in the tyr Z-Mn ensemble) should be, however, contrasted with the NIR-induced oxidation of tyr Z (the charge of the Mn-tyrZ ensemble is preserved), which may not be limited by the same restrictions.

A Molecular Model. The above ideas are incorporated into the molecular model shown in Scheme 2. In addition to one Mn(III) ion two μ-oxo bridged Mn ions are included (the fourth has been omitted). The arrangement and valence assignments of the Mn ions follow those of the model of Siegbahn (*16*), but clearly, this is a schematic illustration, and variant models that do not violate the above criteria can be considered. The sequence of main events in the molecular model of Scheme 2 follows that of Scheme 1. The S_2-to-S_3 transition results in the transfer of an electron to the acceptor side (Q_A, not shown) and a proton to the aqueous phase. The positive hole is assumed to be located on a bridging oxyl radical, as discussed above. Rather than tracing the various paths, as in the description of Scheme 1, we will focus here on certain key intermediates.

An excited S_2 configuration, S_2', is the stable product of charge recombination at cryogenic temperatures and is observed as a signal at $g = 5$. S_2' has the highest spin identified so far in the Mn cluster, $S = {}^7/_2$ (*45*), and following the initial suggestion (*41*), we assign it to a nonprotonated configuration of S_2. This implies that the proton lost upon

the initial S_2-to-S_3 transition is remotely displaced and can be restored only after raising the temperature to about −50 °C. In support of this assignment, S_2' appears to represent an alkaline pH configuration of S_2 stable at -30 °C, as the experiment of Figure 8 in the preceding paper (*26*) suggests.

The precursors to the S_2' state, $S_2'Z^{\bullet}$ and $S_2'Z^-$, are also of particular interest. In both states, the Mn cluster is in a $S = {}^7/_2$ configuration, but with somewhat different crystal field parameters (particular the axial distortion, *D*) from those of the relaxed S_2' at 77K. This is indicated by the $g = 2.9$ resonance which accompanies the common $g = 5$ feature (see, e.g., Figure 7b,c of the preceding paper, *26*, and Figure 6 of the present paper) (*45*). It is reasonable to assume that oxidation of the tyrosine affects charge equilibria in the vicinity and induces proton movements in the cluster resulting in modifications of the crystal field symmetry around the Mn. We show schematically such a movement in the scheme. The proton that forms the hydrogen bond between tyr Z^- and the proximal water in the states S_3 and S_2' is repelled to a distal OH (a direct ligand to Mn) when tyr Z is oxidized (state $S_2'Z^{\bullet}$). This could be the first step of proton translocation under normal circumstances and not easily reversed at liquid He temperatures. This is schematic, of course, and alternative paths cannot be excluded. An attractive alternative would be the transfer of the hydrogen-bonding proton to the bridging oxygen, which is the site of the positive hole in S_3.

In $S_2'Z^{\bullet}$, we also observe in the EPR spectra the signal of the tyrosine, broadened by a weak magnetic interaction with the Mn cluster. The magnetic counter effect of the tyrosine on the broad Mn $S = {}^7/_2$ signal is too weak to be detected.

An $S_2''Z^{\bullet}$ intermediate (the double prime on S_2 is our notation to distinguish from the present S_2' intermediate) has been trapped by a pH jump to alkaline pH of samples in the S_3 state (*63*). S_2'' has been assigned to a doubly deprotonated S_2 configuration of the Mn cluster. No simple comparison can be made with the present S_2' state (assigned to a singly deprotonated configuration of S_2), particularly since the EPR signature of S_2'' is not known yet.

The EPR spectrum of the S_3' state, trapped at 190 K following low-temperature NIR excitation of fresh samples, has components in both parallel and perpendicular mode, but the perpendicular-mode spectrum with a pronounced component at $g = 3.7$ probably originates from a non-true-integer-spin state. It probably arises from the interaction of a radical with a half-integer-spin state of the Mn cluster (a theoretical analysis is currently in progress). The absence of a broadened radical signal in the $g = 2$ region and the presence of a parallel mode component in the spectra indicate that the coupling between the radical and the Mn cluster is stronger than the coupling between tyr Z and the cluster. In the context of the present model, it would be reasonable to position the radical at one of the nonbridging oxygen atoms. According to the calculations of Siegbahn (*16*), water that is not directly bonded to Mn can assist the transfer of the radical character among the oxygens by facilitating the accompanying protonation/deprotonation, with low cost in energy. The transfer of the oxyl character from a bridging to a terminal position has been suggested to be a physiological step during the S_3-to-S_4 transition in certain models (*16*, *17*, *23*). Accordingly, the present results could be an experimental demonstration of such a movement. These considerations could be refined in a number of ways to account for the much higher thermal activation barrier for the S_3*-to-S_3' transition compared with the S_3*-to-$S_2'Z^{\bullet}$ transition (Scheme 1) or the fact that the $S_3'...Q_A^-$ recombination rate appears to be slower than the $S_3...Q_A^-$ rate at 77 K (preliminary unpublished observations). It is possible that these properties reflect constraints imposed by proton reallocation. Finally, various possibilities exist for the precursor to S_3', denoted S_3'' in Scheme 1. One attractive possibility would be that this transient represents a state where the positive hole is on Mn itself. That would be a true-integer-spin state and perhaps EPR-silent.

Scheme 3: Tyr Z as a Proton Repeller/Electron Abstractor

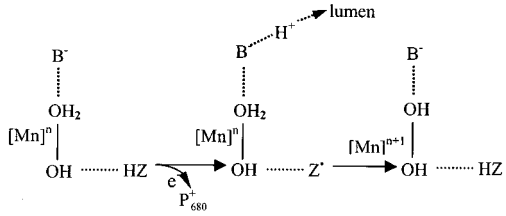

Insights into the Deprotonation Pathway of tyr Z. A Proton Repeller Mechanism. The above considerations indicate an efficient exchange of protons between the Mn cluster and tyr Z. This fact has been recognized earlier (see, e.g., refs *64* and *65*) and, actually, has been the basis of the H-atom (or proton) abstraction mechanism (*10*−*12*). The latter hypothesis assumes that protons removed from the Mn cluster are translocated to the aqueous phase via tyr Z and a subsequent array of proton acceptors. His 190 of the D_1 protein is assumed to be the critical primary proton acceptor. This assignment is based, however, on studies of Mn depleted or inhibited preparations (reviewed in refs *58* and *61*,) and the earlier considerations in this section argued that the efficient proton acceptors in untreated preparations should be associated with the Mn cluster itself.

An alternative hypothesis is outlined in Scheme 3. We assume that water associated with the Mn cluster is in hydrogen-bonding contact with tyr Z. An array comprising this water and adjacent water (or OH or O) ligands to Mn followed by a sequence of proton acceptors acts as an efficient proton translocation pathway under normal circumstances. Alternative bases in the vicinity would contribute to the extent of de-protonation, but their role becomes of primary significance only in cases of deficiency of the Mn cluster. Oxidation of tyr Z therefore repels the hydrogen-bonding proton toward the cluster and initiates proton translocation via the cluster. This first step in Scheme 3 describes tyr Z as a proton repeller, and it is entirely consistent with the experimental observation that, proton release during S-state turnover precedes the actual S-state transitions being correlated with P_{680}^+ reduction and tyr Z oxidation, rather than with tyr Z reduction (*20*, *57*−*59*). The second step in Scheme 3, the reduction of Tyr $Z^{\bullet}$ by the Mn cluster can be viewed as an electron/proton or hydrogen atom abstraction.

In conclusion, the present work places the observations of this and the accompanying paper in a comprehensive order and on a molecular framework. The main intermediates induced by the low-temperature NIR excitation of the S_3 state are attributed to the transfer of the positive hole to different

oxygen ligands of Mn (or to Mn itself) and to tyr Z, accompanied by proton rearrangements. The observations support an intimate relation between tyr Z and the Mn cluster. The proposal that oxidation of tyr Z repels protons to and out from the Mn cluster may be viewed as bridging the two main extreme views in the literature.

ACKNOWLEDGMENT

We thank Dr. Y. Sanakis for helpful discussions and Mr. P. Tampourlos for technical help. N.I. thanks I.K.Y. (Greek State Scholarship Foundation) for financial support.

REFERENCES

1. Diner, B. A., and Babcock, G. T. (1996) in *Advances in Photosynthesis: Vol. 4. Oxygenic Photosynthesis: The Light Reactions* (Ort, R. D., and Yocum, C. F., Eds.) pp 213−247, Kluwer Academic Publishers, Dordrecht, The Netherlands.
2. Diner, B. A., Petrouleas, V., and Wendoloski, J. J. (1991) *Physiol. Plant. 81*, 423−436.
3. Debus, R. J. (1992) *Biochim. Biophys. Acta 1102*, 269−352.
4. Bricker, T. M., and Ghanotakis, D. F. (1996) in *Advances in Photosynthesis: Vol. 4. Oxygenic Photosynthesis: The Light Reactions* (Ort, R. D., and Yocum, C. F., Eds.) pp 113−136, Kluwer Academic Publishers, Dordrecht, The Netherlands.
5. Britt, R. D. (1996) in *Advances in Photosynthesis: Vol. 4. Oxygenic Photosynthesis: The Light Reactions* (Ort, R. D., and Yocum, C. F., Eds.) pp 137−164, Kluwer Academic Publishers, Dordrecht, The Netherlands.
6. Robblee, J. H., Cinco, R. M., and Yachandra, V. K. (2001) *Biochim. Biophys. Acta 1503*, 7−23.
7. Brudvig, G. W., and Crabtree, R. H. (1986) *Proc. Natl. Acad. Sci. U.S.A. 8*3, 4586−4588.
8. Christou, G., and Vincent, J. B. (1987) *Biochim. Biophys. Acta 89*5, 259−274.
9. Pecoraro, V. L. (1992) in *Manganese Redox Enzyme*s (Pecoraro, V. L., Ed.) pp 197−231, VCH Publishers, New York.
10. Gilchrist, M. L., Ball, J. A., Randall, D. W., and Britt, R. D. (1995) *Proc. Natl. Acad. Sci. U.S.A. 92*, 9545−9549.
11. Hoganson, C. W., Lydakis-Simantiris, N., Tang, X.-S., Tommos, C., Warncke, K., Babcock, G. T., Diner, B. A., McCracken, J. and Styring, S. (1995) *Photosynth. Res. 46*, 177−184.
12. Hoganson, C. W., and Babcock, G. T. (1997) *Science 277*, 1953−1956.
13. Haumann, M., and Junge, W. (1999) *Biochim. Biophys. Acta 1411*, 86−91.
14. Schlodder, E., and Witt, H. T. (1999) *J. Biol. Chem.*, *274*, 30387−30392.
15. Siegbahn, P. E. M., and Crabtree, R. H. (1999) *J. Am. Chem. Soc.*, *121*, 117−127.
16. Siegbahn, P. E. M. (2000) *Inorg. Chem. 39*, 2923−2935.
17. Messinger, J. (2000) *Biochim. Biophys. Acta*, *1459*, 481−488.
18. Renger, G. (2001) *Biochim. Biophys. Acta 1503*, 210−228.
19. Dau, H., Luzzolino, L. and Dittmer, J. (2001) *Biochim. Biophys. Acta 1503*, 24−39.
20. Nugent, J. H. A., Rich, A. M., and Evans, M. C. W. (2001) *Biochim. Biophys. Acta 1503*, 138−146.
21. Hillier, W., and Wydrzynski T. (2001) *Biochim. Biophys. Acta 1503*, 197−209.
22. Vrettos, J. S., Limburg, J., and Brudvig, G. W. (2001) *Biochim. Biophys. Acta 1503*, 229−245.
23. Messinger, J., Robblee, J. H., Bergmann, U., Fernandez, C., Glatzel, P., Visser, H., Cinco, R. M., McFarlane, K. L., Bellacchio, E., Pizarro, S. A., Cramer, S. P., Sauer, K., Klein, M. P., and Yachandra, V. K. (2001) *J. Am. Chem. Soc. 123*, 7804−7820.
24. Carrel, T. G., Tyryshkin, A. M., and Dismukes, G. C. (2002) *J. Biol. Inorg. Chem. 7*, 2−22.
25. Zouni, A., Witt, H. T., Kern. J., Fromme, P., Krauss, N., Saenger, W., and Orth, P. (2001) *Nature 409*, 739−743.
26. Ioannidis, N. and Petrouleas, V. (2002) *Biochemistry 41*, 9580−9588.
27. Boussac, A., Zimmermann, J. L., and Rutherford, A. W. (1989) *Biochemistry 28*, 8984−8989.
28. Sivaraja, M., Tso, J., and Dismukes, G. C. (1989) *Biochemistry 28*, 9459−9464.
29. Ono, T., and Inoue, Y. (1990) *Biochim. Biophys. Acta 1020*, 269−277.
30. Baumgarten, M., Philo, J. S., and Dismukes, G. C. (1990) *Biochemistry 29*, 10814−10822.
31. Andreasson, L.-E., and Lindberg, K. (1992) *Biochim. Biophys. Acta 1100*, 177−183.
32. Hallahan, B. J., Nugent, J. H. A., Warden, J. T. and Evans, M. C. W. (1992) *Biochemistry 31*, 4562−4573.
33. MacLachlan, D. J., and Nugent, J. H. A. (1993) *Biochemistry 32*, 9772−9780.
34. Szalai, V. A., and Brudvig, G. W. (1996) *Biochemistry 35*, 1946−1953.
35. Astashkin, A. V., Mino, H. Kawamori, A., and Ono, T. (1997) *Chem. Phys. Lett. 272*, 506−516.
36. Tang, X.-S., Randall, D. W., Force, D. A., Diner, B. A., and Britt, R. D. (1996) *J. Am. Chem. Soc. 118*, 7638−7639.
37. MacLachlan, D. J., Nugent, J. H. A., Warden, J. T., and Evans, M. C. W. (1994) *Biochim. Biophys. Acta 1188*, 325−334.
38. Peloquin, J. M., Campbell, K. A., and Britt, R. D. (1998) *J. Am. Chem. Soc. 120*, 6840−6841.
39. Dorlet, P., Di Valentin, M., Babcock, G. T., and McCracken, J. L. (1998) *J. Phys. Chem. B 102*, 8239−8247.
40. Lakshmi, K. V., Eaton, S. S., Eaton, G. R., Frank, H. A., and Brudvig, G. W. (1998) *J. Phys. Chem. B 102*, 8327−8335.
41. Nugent, J. H. A., Turconi, S., and Evans, M. C. W. (1997) *Biochemistry 36*, 7086−7096.
42. Ioannidis, N., and Petrouleas, V. (2000) *Biochemistry 39*, 5246−5254.
43. Boussac, A., Girerd, J.-J., and Rutherford, A. W. (1996) *Biochemistry 35*, 6984−6989.
44. Boussac, A., Un, S., Horner, O., and Rutherford, A. W. (1998) *Biochemistry 37*, 4001−4007.
45. Sanakis, Y., Ioannidis, N., Sioros, G., and Petrouleas, V. (2001) *J. Am. Chem. Soc. 123*, 10766−10767.
46. Berthold, D. A., Babcock, G. T., and Yocum, C. F. (1981) *FEBS Lett. 134*, 231−234.
47. Ford R. C., and Evans, M. C. W. (1983) *FEBS Lett. 160*, 159−164.
48. Matsukawa, T., Mino, H., Yoneda, D., and Kawamori, A. (1999) *Biochemistry 38*, 4072−4077.
49. Nugent, J. H. A., Muhiuddin, I. P., and Evans, M. C. W. (2002) *Biochemistry 41*, 4117−4126.
50. Baxter, R., Krausz, E., Wydrzynski, T., and Pace, R. J. (1999) *J. Am. Chem. Soc. 121*, 9451−9452.
51. Peloquin, J. M., Campbell, K. A., Randall, D. W., Evanchik, M. A., Pecoraro, V. L., Armstrong, W. H., and Britt, R. D. (2000) *J. Am. Chem. Soc. 122*, 10926−10942.
52. Roelofs, T. A., Liang, W., Latimer, M. J., Cinco, R. M., Rompel, A., Andrews, J. C., Sauer, K., Yachandra, V. K., and Klein, M. (1996), *Proc. Natl. Acad. Sci. U.S.A. 9*3, 3335−3340.
53. Ono, T. A., Noguchi, T., Inoue, Y., Kusunoki, M., Matsushita, T., and Oyanagi, H. (1992) *Science 25*8, 1335−1337.
54. Iuzzolino, L., Dittmer, J., Dorner, W., Meyer-Klaucke, W., and Dau, H. (1998), *Biochemistry 37*, 17112−17119.
55. Ioannidis, N., Schansker, G., Barynin, V. V., and Petrouleas, V. (2000) *JBIC, J. Biol. Inorg. Chem. 5*, 354−363.
56. Messinger, J., and Renger, G. (1990) *FEBS Lett. 277*, 141−146.
57. Haumann, M., and Junge, W. (1996) in *Advances in Photosynthesis: Vol. 4. Oxygenic Photosynthesis: The Light Reactions* (Ort, R. D., and Yocum, C. F., Eds.) pp 165−192, Kluwer Academic Publishers, Dordrecht, The Netherlands.
58. Diner, B. A. (2001) *Biochim. Biophys. Acta 1503*, 147−163.
59. Rappaport, F., and Lavergne, J. (2001) *Biochim. Biophys. Acta 1503*, 246−259.
60. Rappaport, F., Blanchard-Desce, M. and Lavergne, J. (1994) *Biochim. Biophys. Acta 1184*, 178−192.
61. Debus, R. J. (2001) *Biochim. Biophys. Acta 1503*, 164−186.
62. Nugent, J. H. A. (1996) *Eur. J. Biochem. 237*, 519−531.
63. Geijer, P., Morvaridi, F., and Styring, S. (2001) *Biochemistry 40*, 10881−10891.
64. Noguchi, T., Inoue, Y., and Tang, X. S. (1997) *Biochemistry 36*, 14705−14711.
65. Szalai, V. A., Kuhne, H., Lakhsmi, K. V., and Brudvig, G. W. (1998) *Biochemistry 37*, 13594−13603.

BI0159940